Chemical Physics 391 (2011) 101–109

Contents lists available at ScienceDirect

Chemical Physics

journal homepage: www.elsevier.com/locate/chemphys

Nonadiabatic molecular dynamics with solvent effects: A LR-TDDFT QM/MM study of ruthenium (II) tris (bipyridine) in water

Ivano Tavernelli *, Basile F.E. Curchod, Ursula Rothlisberger

Laboratory of Computational Chemistry and Biochemistry, Ecole Polytechnique Fédérale de Lausanne, CH-1015 Lausanne, Switzerland

ARTICLE INFO

Article history:
Available online 30 March 2011

Keywords:
LR-TDDFT
QM/MM
Surface hopping
Nonadiabatic dynamics
Ruthenium (II) tris (bipyridine)
Inorganic dyes

ABSTRACT

The previously derived trajectory-based nonadiabatic molecular dynamics scheme [E. Tapavicza, I. Tavernelli, U. Rothlisberger, Phys. Rev. Lett. 98 (2007) 023001] is extended to include the coupling of the quantum system with a classically described environment. The dynamics is performed using LR-TDDFT energies and forces computed on-the-fly together with the nonadiabatic coupling vectors needed for the propagation of the nuclear coefficients according to Tully's fewest-switches surface hopping algorithm. The resulting LR-TDDFT-QM/MM approach is applied to the study of the ultrafast relaxation of the photoexcited singlet metal-to-ligand-charge-transfer state (^{1}MLCT) of $[Ru(bpy)_3]^{2+}$ (bpy = 2,2′-bipyridine) in water. The observed intersystem crossing dynamics with the triplet MLCT is in good agreement with available experimental results.

1. Introduction

In recent years, the calculation of excited states energies and properties of medium to large molecular systems has received an important boost thanks to the development and the efficient implementation of linear response time-dependent density functional theory (LR-TDDFT) [1–5]. Alternative wavefunction-based approaches like the complete active space self-consistent field (CASSCF) method (often supplemented with perturbation of second order (CASPT2) or configuration interaction with single and double excitations (MR-CISD) [6]) are also available but their application in the study of photochemical and photophysical processes is still hampered by their intrinsic limitations (construction and size of the active space) and their computational costs. On the other end, single reference methods like second-order approximate coupled cluster singles and doubles (CC2) are valid possible alternatives to LR-TDDFT for the calculation of accurate potential energy surfaces (PESs) of medium size molecular systems [7,8].

Despite its conceptual simplicity, LR-TDDFT is far from being a "black-box" tool for the calculation of excited state properties. In fact, even though TDDFT is in principle an exact theory, practical numerical calculations rely on a number of approximations that can decrease in a more or less unpredictable way the accuracy of its predictions. The most important are the approximation of the exchange and correlation (*xc*) functional and the use of the so-called adiabatic approximation in the evaluation of the TDDFT kernel [9–11]. Their effect is particularly strong in the calculation of charge transfer (CT) states of molecular systems for which the LR-TDDFT energies are in general severely underestimated. However, long-range corrected *xc*-functionals like for instance CAM-B3LYP [12] and LC-ωPBE [13,14] or meta-hybrid functionals such as M06-2X [15,16] have dramatically improved the description of these excitations [8,17–19].

Despite these potential failures, LR-TDDFT is the method of choice to combine with nonadiabatic molecular dynamics techniques when the quality of the PESs is sufficiently good. In fact, the availability of analytic gradients in LR-TDDFT [20,21] offers a very efficient way for the on-the-fly calculation of the nuclear forces. The coupling of LR-TDDFT with nonadiabatic dynamics schemes like Landau–Zener dynamics [22–24], Tully's trajectory surface hopping [25], Ehrenfest dynamics [26], and Bohmian dynamics [27], has already shown the validity of this approach in the description of a number of different photochemical and photophysical processes [28–32]. In addition, the coupling of DFT and LR-TDDFT electronic structure calculations with a classical (molecular mechanics, MM) description of the environment offers the possibility to investigate the effects of the solvent (or of a more complex environment like a protein matrix) on the reaction dynamics. An extension of the so-called quantum mechanics/molecular mechanics (QM/MM) formalism to excited states is particularly simple in the framework of LR-TDDFT since the coupling with the classical point charges of the environment only requires the knowledge of the excited state density, which is easily accessible in LR-TDDFT calculations.

The implementation of a nonadiabatic molecular dynamics scheme requires however the calculation of additional electronic structure properties that are not simple functionals of the

* Corresponding author.
E-mail address: ivano.tavernelli@epfl.ch (I. Tavernelli).

0301-0104/$ - see front matter © 2011 Elsevier B.V. All rights reserved.
doi:10.1016/j.chemphys.2011.03.021

electronic density. In particular, nonadiabatic coupling elements (NACs) and nonadiabatic coupling vectors (NACVs), which describe the coupling of different excited electronic states through the nuclear motion, are naturally formulated in terms of the many-electron wavefunctions. Nevertheless, several schemes for the calculation of NACVs within TDDFT are nowadays available, provided that one of the states is the ground state. Chernyak and Mukamel [33] were the first to give an explicit formula for the NACVs within the TDDFT density-matrix approach, followed by the work of Baer [34] based on real-time TDDFT and the study of nonadiabatic effects in the context of vibronic couplings by Neugebauer and coworkers [9,35]. Later, Tavernelli et al. [36–38] and Hu et al. [39] independently suggested an additional solution to the problem using Casida's formulation of the LR-TDDFT equations. Our approach, which is based on a reconstruction of an auxiliary many-electron wavefunction, was first validated in the case of NACVs involving the ground state [40], and subsequently extended to the calculation of couplings between any pair of excited states with the same spin multiplicity [41].

This article is organized in the following way. After a short review on the coupling of LR-TDDFT with trajectory surface hopping dynamics and on the calculation of NACVs within LR-TDDFT, we give a description of the Hamiltonian coupling term used to couple the classical environment (MM subsystem) with the LR-TDDFT electronic density of the quantum (QM) subsystem. The method is then applied to the study of the fast excited state dynamics of $[Ru(bpy)_3]^{2+}$ (bpy = 2,2′-bipyridine) in water after photoexcitation into a singlet metal-to-ligand-charge-transfer (MLCT) state. The intersystem crossing (ISC) with the lower lying triplet states is discussed and provides a theoretical description of the experimentally observed ultrafast singlet to triplet MLCT conversion.

2. Theory

2.1. Trajectory surface hopping within LR-TDDFT

Trajectory surface hopping [25] (TSH) is one of the most widely used methods for the simulation of nonadiabatic processes beyond the Born–Oppenheimer approximation. The dynamics of the nuclei occurs on adiabatic PESs computed at a chosen level of theory (*ab initio* or semi-empirical) and follows classical trajectories with the exception of "quantum hops" between PESs induced by large values of the nonadiabatic couplings. It is worth mentioning that due to the classical nature of the nuclear dynamics, effects like quantum decoherence and nuclear tunneling are not captured by this approximation (see Refs. [42–45] for a careful analysis of TSH).

In practice, the nuclear dynamics is represented by a swarm of independent (not correlated) trajectories started from a thermal distribution of initial conditions (positions and momenta). To each of these trajectories (labelled by the index α) we associate time-dependent amplitudes $C_J^\alpha(t)$ for each PES J. These amplitudes correspond to the time-dependent coefficients of the molecular wavefunction expansion

$$\Psi^\alpha(\boldsymbol{r},\boldsymbol{R},t)=\sum_J^\infty C_J^\alpha(t)\Phi_J(\boldsymbol{r};\boldsymbol{R}) \tag{1}$$

in a complete basis of adiabatic electronic states $\Phi_J(\boldsymbol{r};\boldsymbol{R})$. Here and in the following equations $\boldsymbol{R}$ and $\boldsymbol{r}$ represent the collective coordinates of all nuclei, and electrons respectively. When inserted into the time-dependent Schrödinger equation one obtains the following set of coupled equations for the amplitudes associated with the different PESs

$$i\hbar\dot{C}_J^\alpha(t)=\sum_I C_I^\alpha(t)\left(H_{JI}-i\hbar\dot{\boldsymbol{R}}^\alpha\cdot\boldsymbol{d}_{JI}^\alpha\right). \tag{2}$$

In the adiabatic representation of the electronic wavefunctions, the off-diagonal matrix elements $H_{JI}=\langle\Phi_J|\mathcal{H}_{el}|\Phi_I\rangle$ are equal to zero, whereas the diagonal terms are simply the eigenvalues of the electronic time-independent Schrödinger equation for a nuclear configuration $\boldsymbol{R}$, $H_{JJ}=E_J^{el}(\boldsymbol{R})$.

All matrix elements in Eq. (2) are computed using a suitable *ab initio* electronic structure method. In our implementation of TSH we use density functional theory for the ground state and linear response time-dependent density functional theory for the excited state energies $E_J^{el}(\boldsymbol{R})$ and couplings $\boldsymbol{d}_{JI}^\alpha(\boldsymbol{R})$ (see Refs. [36,38,46] for a detailed description of TSH implementation in the plane wave software package CPMD [47]).

In Tully's "fewest-switches" TSH algorithm [25], the classical trajectories evolve adiabatically according to Born–Oppenheimer dynamics until a *hop* between two PESs (H_{II} and H_{JJ}) occurs with a probability given by a Monte Carlo-type criterion. The transition probability from state I to state J in the time interval $[t,t+dt]$ is given by

$$g_{IJ}^\alpha(t,t+dt)=2\int_t^{t+dt}d\tau\frac{Im\left[C_J^\alpha(\tau)C_I^{\alpha*}H_{JI}(\tau)\right]-Re\left[C_J^\alpha(\tau)C_I^{\alpha*}(\tau)\Xi_{JI}^\alpha(\tau)\right]}{C_I^\alpha(\tau)C_I^{\alpha*}(\tau)}, \tag{3}$$

where $\Xi_{JI}^\alpha(\tau)=\dot{\boldsymbol{R}}^\alpha\cdot\boldsymbol{d}_{JI}^\alpha(\tau)$, and a hop occurs if and only if

$$\sum_{K\leqslant J-1}g_{IK}^\alpha<\zeta<\sum_{K\leqslant J}g_{IK}^\alpha, \tag{4}$$

where ζ is generated randomly in the interval $[0,1]$. The final statistical distribution of all trajectories is assumed to reproduce the correct probability density distribution of the nuclear wavepacket. It is important to stress that, at present, no formal justification of Tully's algorithm has been formulated.

2.2. Nonadiabatic coupling vectors between excited states

In this chapter we will briefly summarize the method used to compute the NACVs within LR-TDDFT. The NACVs between two electronic states I and J at a given nucleus γ, $\boldsymbol{d}_{IJ,\gamma}$, are formally given by the respective many-electron wavefunctions $\boldsymbol{\Phi}_I$ and $\boldsymbol{\Phi}_J$:

$$\boldsymbol{d}_{IJ,\gamma}=\langle\Phi_I|\nabla_\gamma|\Phi_J\rangle=\frac{\langle\Phi_I|\nabla_\gamma\mathcal{H}_{el}|\Phi_J\rangle}{E_J-E_I}, \tag{5}$$

where here ∇_γ designed the nuclear gradient with respect to nuclei γ. Recently, we showed that within LR-TDDFT any matrix element of a general one-body operator $\mathcal{O}$ can be written with the help of a set of auxiliary many-electron wavefunctions defined as (for the excited state I)

$$|\widetilde{\Psi}_I\rangle=\sum_{ia}c_{ia}^I\hat{c}_a^\dagger\hat{c}_i|\widetilde{\Psi}_0\rangle, \tag{6}$$

where ia denotes a single excitation from the occupied Kohn–Sham (KS) orbital i to the virtual orbital a, $\hat{c}_a^\dagger$ and $\hat{c}_i$ are the corresponding creation and annihilation operators, $|\widetilde{\Psi}_0\rangle$ is the ground state KS Slater determinant, and $c_{ia}^I=\sqrt{\frac{\epsilon_a-\epsilon_i}{\Omega_I}}e_{ia}^I$ are coefficients entirely determined by LR-TDDFT quantities such as the energy eigenvalues Ω_I with corresponding eigenvectors e_{ia}^I and the KS energy differences $(\epsilon_a-\epsilon_i)$ [37,38,40]. We use the following convention for the molecular orbitals indices: $\{i,j,\ldots\}$ = occupied; $\{a,b,\ldots\}$ = unoccupied; $\{p,q,\ldots\}$ = either occupied or unoccupied.

Matrix elements of one-body operators involving the ground state can then be computed using

$$\begin{aligned}\sigma_{0I}&=\sum_{ia}c_{ia}^I\left\langle\widetilde{\Psi}_0|\mathcal{O}|\widetilde{\Psi}_{i\to a}\right\rangle=\sum_{ia}c_{ia}^I\langle\phi_i|\mathcal{O}|\psi_a\rangle\\&=\sum_{ia}\sqrt{\frac{\epsilon_a-\epsilon_i}{\Omega_I}}e_{ia}^I\langle\phi_i|\mathcal{O}|\psi_a\rangle,\end{aligned} \tag{7}$$

where $\widetilde{\Psi}_{i\to a}$ is the obvious notation for the auxiliary many-electron wavefunctions obtained from the one-electron excitation $i \to a$, and $\{\phi_{i\sigma}(\mathbf{r})\}_{i=1}^{N}$ and $\{\psi_{a\sigma}(\mathbf{r})\}_{a=1}^{\infty}$ are the occupied and virtual KS orbitals, respectively, with corresponding occupations $f_i = 1$ and $f_a = 0$.

Using the equality $e^I_{ia} = \sqrt{\Omega_I}[(A-B)^{-1/2}(X_I+Y_I)]_{ia}$ between the LR-TDDFT eigenvectors e^I_{ia} and the (ph,hp) solutions of Casida's equations [3] (X_I, Y_I) we finally obtain

$$\sigma_{0I} = \sum_{ia}(X_I+Y_I)_{ia}\langle\phi_i|\mathcal{O}|\psi_a\rangle = \sum_{ia}(X_I+Y_I)_{ia}\mathcal{O}^T_{ai}, \tag{8}$$

where $\mathcal{O}_{ia} = \langle\phi_i|\mathcal{O}|\psi_a\rangle$.

The same approach can also be used for the calculation of matrix elements between two excited states [41]. In this case we obtained

$$\begin{aligned}\sigma_{IJ} &= \sum_{ia}\sum_{jb} c^{I\dagger}_{ia}c^J_{jb}\langle\widetilde{\Psi}_{i\to a}|\mathcal{O}|\widetilde{\Psi}_{j\to b}\rangle \\ &= \sum_{iab} c^{I\dagger}_{ia}c^J_{ib}\langle\psi_a|\mathcal{O}|\psi_b\rangle - \sum_{aij} c^{I\dagger}_{ia}c^J_{ja}\langle\phi_i|\mathcal{O}|\phi_j\rangle,\end{aligned} \tag{9}$$

which matches exactly the leading linear response contribution $\sigma_{I,J}$ obtained with the second-order coupled electronic oscillator approach of Mukamel and coworkers [48] and becomes exact within the Tamm–Dancoff approximation (TDA) [49,41]. In terms of Casida's eigenvectors (X_I, Y_I) we finally obtain

$$\begin{aligned}\sigma_{I,J} = &\sum_{ab}\left(X^\dagger_I X_J + X^\dagger_I Y_J + Y^\dagger_I X_J + Y^\dagger_I Y_J\right)_{ab}\langle\psi_b|\mathcal{O}|\psi_a\rangle \\ &- \sum_{ij}\left(X_J X^\dagger_I + Y_J X^\dagger_I + X_J Y^\dagger_I + Y_J Y^\dagger_I\right)_{ji}\langle\phi_i|\mathcal{O}|\phi_j\rangle.\end{aligned} \tag{10}$$

The calculation of the NACVs is performed for $\mathcal{O} = \nabla_\gamma \mathcal{H}_{el}$. Implementation of the couplings in the plane wave DFT code CPMD is given in full details in Ref. [37].

2.3. The LR-TDDFT/MM coupling Hamiltonian

In this Section we briefly summarize the basic principles of the QM/MM method and present an extension for the coupling of an excited electronic density with classical atoms of the environment. A complete discussion of the QM/MM methodology for electronic ground state can be found in Refs. [50–52].

The QM/MM approach is based on the partitioning of the system into two subsystems: a "central" quantum region described at an *ab initio* or semi-empirical level (here DFT and LR-TDDFT) and a surrounding environment described at a molecular mechanical (force field) level.

In this work we use an additive scheme, which is based on the total Hamiltonian [51]

$$H_{tot} = H_{QM} + H_{MM} + H_{QM/MM}, \tag{11}$$

where H_{QM} is the quantum Hamiltonian, H_{MM} is the classical Hamiltonian, and $H_{QM/MM}$ is the Hamiltonian describing the coupling between the QM and the MM part of the system. Within this scheme, we explicitly take into account the effect of the MM atoms on the QM system (polarization of the electronic density). It is however important to note here that the back-reaction of the QM system to the MM system would require a polarizable force field and is not taken into account.

The interaction energy between the QM and the MM is given by

$$\begin{aligned}E_{QM/MM} = &\sum_\gamma q_\gamma \int v_{sC}(|\boldsymbol{R}_\gamma - \mathbf{r}|)\rho_0(\mathbf{r})d\mathbf{r} + \sum_{\gamma'\gamma}\frac{Z_{\gamma'}q_\gamma}{|\boldsymbol{R}_{\gamma'} - \boldsymbol{R}_\gamma|} \\ &+ \frac{1}{2}\sum_{\gamma'}\sum_{\gamma} 4\epsilon_{\gamma'\gamma}\left(\left(\frac{\sigma_{\gamma'\gamma}}{|\boldsymbol{R}_\gamma - \boldsymbol{R}_{\gamma'}|}\right)^{12} - \left(\frac{\sigma_{\gamma'\gamma}}{|\boldsymbol{R}_\gamma - \boldsymbol{R}_{\gamma'}|}\right)^{6}\right),\end{aligned} \tag{12}$$

where the first two terms represent the electrostatic interaction of the QM subsystem (electronic density, $\rho_0(\mathbf{r})$, and the nuclear charges, $Z_{\gamma'}$) with the point charges of the classical (MM) part, q_γ, and the third term describes the van der Waals (vdW) interactions between QM atoms and MM atoms (E^{vdW}). The potential $v_{sC}(|\boldsymbol{R}_\gamma - \mathbf{r}|)$ is a screened Coulomb potential generated by the atom at $\boldsymbol{R}_\gamma$ and modified at short range in order to avoid spurious overpolarization effects [51]

$$v_{sC}(|\boldsymbol{R}_\gamma - \mathbf{r}|) = \frac{r_C^4 - (|\boldsymbol{R}_\gamma - \mathbf{r}|)^4}{r_C^5 - (|\boldsymbol{R}_\gamma - \mathbf{r}|)^5}, \tag{13}$$

where r_C is the covalent radius of atom γ. In Eq. (12) the index γ labels MM atoms while γ' runs over atoms in the QM region. All parameters are part of the classical force field used for the classical MM part (q_γ: classical charge associated to atom γ, $\epsilon_{\gamma'\gamma}$: are the energy minima of the vdW potential for the pair (γ,γ'), $\sigma_{\gamma'\gamma}$: corresponding vdW parameters). For reasons of numerical efficiency, the electrostatic interaction between the QM system and the more distant MM atoms (outside a cutoff distance d_c from any QM atom) is included via a Hamiltonian term explicitly coupling the multiple moments of the quantum charge distribution with the classical point charges [51].

In LR-TDDFT the electronic density is perturbed by the interaction with the external time-dependent perturbation field $v_{pert}(\mathbf{r},t)$ and, within linear response, we have

$$\delta\rho(\mathbf{r},t) = \int dt' \int d\mathbf{r}'\chi(\mathbf{r},t,\mathbf{r}',t')v_{pert}(\mathbf{r}',t'), \tag{14}$$

where $\chi(\mathbf{r},t,\mathbf{r}',t')$ is the density response function of the system defined as

$$\chi(\mathbf{r},t,\mathbf{r}',t') = \left.\frac{\delta\rho(\mathbf{r},t)}{\delta v_{ext}(\mathbf{r}',t')}\right|_{v_0}, \tag{15}$$

$v_0(\mathbf{r})$ is the ground state KS potential, and $v_{ext}(\mathbf{r},t) = v_0(\mathbf{r}) + v_{pert}(\mathbf{r},t)$. The response function for the physical system of interacting electrons, $\chi(\mathbf{r},t,\mathbf{r}',t')$, can be related to the computationally more advantageous Kohn–Sham response, $\chi_s(\mathbf{r},t,\mathbf{r}',t')$, through the Dyson-like equation

$$\begin{aligned}\chi(\mathbf{r},t,\mathbf{r}',t') = \chi_s(\mathbf{r},t,\mathbf{r}',t') + \int dt_1\int d\mathbf{r}_1\int dt_2\int d\mathbf{r}_2 \\ \times\chi_s(\mathbf{r},t,\mathbf{r}_1,t_1)\frac{\delta v_{Hxc}(\mathbf{r}_1,t_1)}{\delta\rho(\mathbf{r}_2,t_2)}\chi(\mathbf{r}_2,t_2,\mathbf{r}',t'),\end{aligned} \tag{16}$$

where $f_{xc}(\mathbf{r}_1,t_1,\mathbf{r}_2,t_2) = \frac{\delta v_{xc}(\mathbf{r}_1,t_1)}{\delta\rho(\mathbf{r}_2,t_2)}$ is the LR-TDDFT exchange–correlation kernel and $v_{Hxc} = v_H + v_{xc}$. Within the so-called adiabatic approximation [4,3]

$$f_{xc}[\rho](\mathbf{r}_1,t_1,\mathbf{r}_2,t_2) = \delta(t_2-t_1)\frac{\delta E_{xc}[\rho]}{\delta\rho(\mathbf{r}_1)\delta\rho(\mathbf{r}_2)}, \tag{17}$$

where $\rho(\mathbf{r})$ is evaluated at time $t_1 = t_2$, Eq. (16) can be inverted and becomes (in frequency space)

$$\begin{aligned}\chi(\mathbf{r},\mathbf{r}',\omega) = &\chi_s(\mathbf{r},\mathbf{r}',\omega) \\ &+ \chi(\mathbf{r},\mathbf{r}',\omega)\left(\frac{1}{|\mathbf{r}-\mathbf{r}'|} + f_{xc}(\mathbf{r},\mathbf{r}')\right)\chi_s(\mathbf{r},\mathbf{r}',\omega)\end{aligned} \tag{18}$$

with the KS density response function

$$\chi_s(\mathbf{r},\mathbf{r}',\omega) = \sum_{pq}(f_q - f_p)\frac{\xi_p(\mathbf{r})\xi^*_q(\mathbf{r})\xi_q(\mathbf{r}')\xi^*_p(\mathbf{r}')}{\omega - (\varepsilon_p - \varepsilon_q) + i\eta}, \tag{19}$$

where η is a positive infinitesimal and f_p is the occupation number of the KS state p. The indices p and q run over all KS orbitals (occupied and virtual) and $\{\xi_p(\mathbf{r})\} = \{\phi_1(\mathbf{r}),\ldots,\phi_N(\mathbf{r}), \psi_1(\mathbf{r}), \psi_2(\mathbf{r})\ldots\}$ (N is the number of occupied KS states).

Eq. (18) combined with Eq. (14) gives, for a given excited state energy Ω_I, the desired perturbation density $\delta\rho_I(\boldsymbol{r})$ to add to the ground state density $\rho_0(\boldsymbol{r})$ and use in the LR-TDDFT/MM coupling Hamiltonian (Eq. (12)) [53].

Within Casida's formulation, the density response $\delta\rho_I(\boldsymbol{r},t)$ can be expanded in the auxiliary many-electron wavefunctions of Eq. (6)

$$\rho_I(\boldsymbol{r},t) = \left\langle \widetilde{\Psi}_I \middle| \sum_{\kappa=1}^{N} \delta(\boldsymbol{r}-\boldsymbol{r}_\kappa) \middle| \widetilde{\Psi}_I \right\rangle = \rho_0(\boldsymbol{r}) + \delta\rho_I(\boldsymbol{r},t), \tag{20}$$

which in first order becomes

$$\begin{aligned}\delta\rho_I(\boldsymbol{r},t) &= \sum_{ia} c_{ia}^I \left\langle \widetilde{\Psi}_0 \middle| \sum_{\kappa=1}^{N} \delta(\boldsymbol{r}-\boldsymbol{r}_\kappa) \middle| \hat{c}_a^\dagger \hat{c}_i \widetilde{\Psi}_0 \right\rangle e^{-i\Omega_I t} + \text{c.c.} \\ &= \sum_{ia} c_{ia}^I \rho'(\boldsymbol{r}) e^{-i\Omega_I t} + \text{c.c.} \\ &= \sum_{pq} f_p \tilde{f}_q c_{pq}^I \rho'(\boldsymbol{r}) e^{-i\Omega_I t} + \text{c.c.}\end{aligned} \tag{21}$$

where N is the number of electrons and $\tilde{f}_p = (1 - f_p)$.

Using the LR-TDDFT equation for the transition density $\rho'(\boldsymbol{r}) = \sum_{pq} f_p \tilde{f}_q (X_I + Y_I)_{pq} \phi_p(\boldsymbol{r}) \psi_q(\boldsymbol{r})$ and the definition of the coefficients c_{pq}^I [36,37,54] we finally get, in agreement with [55,54],

$$\delta\rho_I(\boldsymbol{r}) = \sum_{pq} \Delta P_{pq}^I \xi_p^*(\boldsymbol{r}) \xi_q(\boldsymbol{r}), \tag{22}$$

where

$$\begin{aligned}\Delta P_{pq}^I = &-f_p f_q \left(\sum_a X_{pa}^{I\dagger} X_{qa}^I + \sum_a Y_{qa}^{I\dagger} Y_{pa}^I \right) \\ &+ \tilde{f}_p \tilde{f}_q \left(\sum_i X_{iq}^{I\dagger} X_{ip}^I + \sum_i Y_{ip}^{I\dagger} Y_{iq}^I \right).\end{aligned} \tag{23}$$

In the Sternheimer formulation of LR-TDDFT [56,20,21] the linear response perturbation density is given by

$$\delta\rho_I(\boldsymbol{r},\pm\Omega) = \sum_i \phi_i(\boldsymbol{r}) \left(\phi_{I,i}^{\{\pm\}}(\boldsymbol{r}) \right)^* + \phi_{I,i}^{\{\pm\}}(\boldsymbol{r}) \phi_i^*(\boldsymbol{r}), \tag{24}$$

where the linear response orbitals $\left\{ \phi_{I,i}^{\{\pm\}}(\boldsymbol{r}) \right\}$ satisfy the equation [21]

$$\sum_{j=1}^{N} (\mathcal{H}_0 \delta_{ij} - \epsilon_{ij}) \left| \phi_{I,j}^{\{\pm\}} \right\rangle + \mathcal{Q} \delta v_{I,\text{SCF}}(\pm\Omega) |\phi_i\rangle = \mp\Omega_I \left| \phi_{I,i}^{\{\pm\}} \right\rangle, \tag{25}$$

$\mathcal{Q} = 1 - \sum_{i=1}^{N} |\phi_i\rangle\langle\phi_i|$, $\mathcal{H}_0$ is the Kohn–Sham Hamiltonian, ϵ_{ij} is a Lagrangian multiplier ensuring the orthogonality of the ground state orbitals, and $\delta v_{I,\text{SCF}}(\pm\Omega)$ is the change of self-consistent field (in the adiabatic approximation) upon perturbation

$$\delta v_{I,\text{SCF}}(\boldsymbol{r},\pm\Omega) = \int d\boldsymbol{r}' \left(\frac{1}{|\boldsymbol{r}-\boldsymbol{r}'|} + \left. \frac{\delta^2 E_{xc}}{\delta\rho(\boldsymbol{r})\delta\rho(\boldsymbol{r}')} \right|_{\rho=\rho_0} \right) \delta\rho_I(\boldsymbol{r}',\pm\Omega). \tag{26}$$

In our implementation of the LR-TDDFT/MM interface Hamiltonian in the software package CPMD [47] we use the total electronic density given by $\rho_I(\boldsymbol{r},\pm\Omega) = \rho_0(\boldsymbol{r}) + \delta\rho_I(\boldsymbol{r},\pm\Omega_I)$. For a detailed account of the implementation see the Appendix and Refs. [21,37].

3. Computational methods

3.1. Equilibration of the QM/MM system

The preparation of the ground state QM/MM setup was described in detail in previous publications [57,58]. In short, a ruthenium (II) tris (bipyridine) ($[Ru(bpy)_3]^{2+}$) complex was first solvated in 3298 TIP3P water molecules with two additional Cl^- counter ions. The system was then equilibrated using classical molecular dynamics at a temperature of 300 K and a pressure of 1 atm. The QM/MM setup consists of the $[Ru(bpy)_3]^{2+}$ complex treated at a DFT/TDDFT level surrounding by the solvent (water molecules and counter ions) described at a classical molecular mechanics level. The electrostatic coupling between the quantum and the classical subsystems was computed using the range-splitting coupling Hamiltonian of Refs. [50,51] with a distance cutoff $d_c = 12$ Å. The system was first relaxed and then gradually warmed up to 300 K starting from an initial temperature of 100 K and keeping the pressure constant at 1 atm. After reaching the target temperature, we started a ground state production run in the NpT ensemble ($T = 300$ K and $p = 1$ atm), from which we then selected the two initial frames to start the excited state dynamics. The system was thermostated using a Nosé–Hoover thermostat with a coupling frequency of 2000 cm^{-1}. All QM/MM simulations were performed using Born–Oppenheimer molecular dynamics.

3.2. DFT and LR-TDDFT calculations

Ground state (DFT) and excited state (LR-TDDFT) calculations were performed using the Becke–Perdew [59,60] (BP) GGA *xc*-functional. Plane waves with a cutoff of 75 Ryd. were used to expand the valence electrons in a box of 18 Å × 18 Å × 18 Å. Core electrons were replaced by norm-conserving pseudopotentials of the Martins–Troullier type [61], which account for scalar relativistic effects. A convergence criteria of 10^{-5} a.u. was used for the optimization of Kohn–Sham orbitals. LR-TDDFT calculations were performed within the Tamm–Dancoff (TDA) approximation, within the adiabatic approximation for the *xc*-kernel.

The quality of LR-TDDFT/BP results was assessed by means of additional calculations with the M06 [15] functional on different molecular geometries extracted from our excited states dynamics. The M06 and BP calculations were performed using the software package Gaussian09 [62], the LANL2DZ basis set for the ruthenium atom, and the 6-311G* basis set for all other atoms. The relative excited state energy differences between the first seven computed singlet excited states agree very well between the two calculations (LR-TDDFT/BP vs. LR-TDDFT/M06), with an average difference of about 0.02 eV. Excited states assignments are also in good agreement and show electronic transitions of exclusively MLCT character (no metal centered states are observed [63]).

Spin orbit couplings (SOCs) were computed with the perturbative approach of Ziegler and coworkers [64] as implemented in the software package ADF2009.01 [65–68]. The calculation was performed on the geometry corresponding to the crossing between states S_2 and T_4 along the first excited state trajectory (see Fig. 2, left panel, $t = 41$ fs). A TZP basis set was used for all atoms and scalar relativistic effects were included using ZORA [69,70]. Water was described by a continuum model using COSMO [71]. The use of an implicit solvation model had the effect of spreading the excited electron over a larger portion of the ligand system, while the changes in the electronic excitations energies are relatively small (RMSD of about 0.15 eV) [72].

All molecular representations are produced with the version 1.8.7 of VMD [73].

3.3. Nonadiabatic dynamics

Nonadiabatic dynamics was performed using the fewest-switches trajectory surface hopping algorithm of Tully [25] as implemented in the plane wave code CPMD [36,38,47]. Nuclear forces were computed according to Ref. [21]. The dynamics was performed in the NpT ensemble using a time step of 5 a.u. At each time step, the first seven excited states were computed using

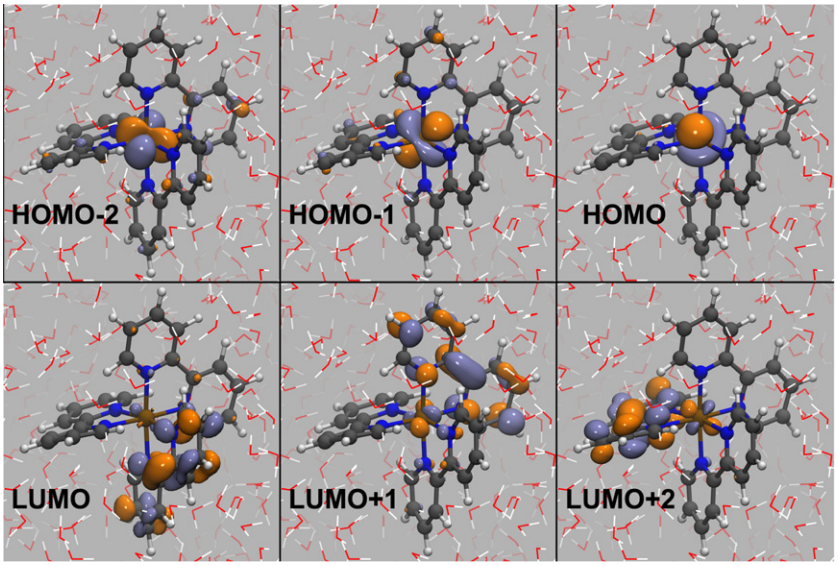

Fig. 1. Selected Kohn–Sham molecular orbitals of a $[Ru(bpy)_3]^{2+}$ complex geometry obtained from the equilibration run. Color code: grey = carbons; blue = nitrogens; white = hydrogens; red = oxygens; ochre = ruthenium (isovalue for the orbitals set to 0.05).

LR-TDDFT/BP/MM in the adiabatic approximation for the *xc*-kernel. Due to the size of the system, the calculation of a large number of trajectories is beyond the possibilities of our current computational resources.

4. Results and discussion

4.1. Nonadiabatic dynamics of $[Ru(bpy)_3]^{2+}$ in aqueous solution

In this Section, we apply the developed LR-TDDFT/MM nonadiabatic dynamics scheme to the investigation of a typical photophysical system, ruthenium (II) tris (bipyridine) ($[Ru(bpy)_3]^{2+}$) in water. Many different experimental [74–77] and theoretical studies (for example Refs. [78,57,79,58]) have been devoted to the study of the ground and excited state behavior of this compound. Experiments showed that after light irradiation the $[Ru(bpy)_3]^{2+}$ complex relaxes within 100 fs from a singlet metal-to-ligand-charge-transfer (^{1}MLCT) to a long-lived triplet state (^{3}MLCT) where the system is trapped for hundreds of picoseconds [77,76]. The dynamics in the triplet MLCT state was the subject of a recent study based on *ab initio* molecular dynamics in water [58]. Here, we report the first steps of this photophysical process, characterized by the nonadiabatic relaxation of the excited ^{1}MLCT complex and its crossing with the lower lying ^{3}MLCT states. Nonadiabatic effects between electronic states of same multiplicity can be fully described using TSH dynamics, where all environmental solvent effects are treated at a classical level.

Concerning the role of the spin–orbit couplings at the crossing between singlet and triplet states, different methodologies based on DFT/LR-TDDFT have already been proposed and implemented [80–82,64,83,84]. However, to the best of our knowledge, no implementation of SOC calculations in an on-the-fly LR-TDDFT based TSH algorithm dynamics has been reported. This would permit the direct description of intersystem crossings (ISCs) in electronically excited inorganic and organometallic compounds and could find important applications for instance in the design of organic light emitting diodes or dye-sensitized solar cell devices [85,86]. Here, we propose a qualitative estimation of the size of the SOCs based on the analysis of the assignments of the excited states involved (see Ref. [87] for a complete discussion on the evaluation of SOC in the context of metal compounds). Since the quantum yield for the ^{1}MLCT/^{3}MLCT ISC is very close to one [76,77], we expect that a simple qualitative analysis of the SOCs between singlet and triplet states is enough to give a first understanding of this process. It has been shown [85,87] that in order to get non-vanishing SOC matrix elements between MLCT states the singlet and triplet excited states need to: (*i*) have the excited π^* orbital localized on the same ligand, and (*ii*) involve metal d-orbitals of different symmetries. This situation leads to matrix elements of the type $\langle {}^1(d'\pi^*)|\hat{H}_{SO}|{}^3(d\pi^*)\rangle$, which are usually large [87] (d and d' represents two 4d(Ru) orbitals from the t_{2g}-like manifold).

If not specified differently, all DFT/LR-TDDFT calculations were performed using the *xc*-functional BP [59,60]. Addition of exact exchange would improve the description of the transition energies, but its use within a plane wave code is still prohibitive. Nevertheless, for this type of system, GGA functionals have shown to give a good agreement with experiments [58], even though a rigid downshift of all energy states is expected.

4.2. Electronic structure of $[Ru(bpy)_3]^{2+}$

The system composed by the ruthenium complex (treated at DFT level) and the solvent (water molecules and counter ions at classical level) are first equilibrated in the NpT ensemble at a temperature of 300 K and a pressure of 1 atm using QM/MM Born–Oppenheimer molecular dynamics. Different structures were then selected to perform the analysis of the excited states and to start the excited state dynamics.

The first singlet excited states of $[Ru(bpy)_3]^{2+}$ are typically assigned to MLCT states [76,77,58], where an electron is excited from a 4d(Ru) orbital to a mainly ligand-based π^* molecular orbital. The highest occupied KS orbitals (KS-HOMO) are mainly of t_{2g}-type symmetry while the lowest unoccupied manifold of KS orbitals are π^*-ligand centered orbitals (Fig. 1). As a consequence, the first vertical excitations show a clear MLCT character (Table 1[1]). Interestingly, the unoccupied orbitals are mainly localized on a single bipyridine ligand. However, due to the mixed character of the LR-TDDFT excitations, the excited electron can become delocalized over different ligands. This behavior is observed for example for the electronic states S_4 and S_6 (see Table 1). It is interesting to note that the

[1] Regarding S_7, LUMO + 3 is also a π^* orbital localized on one of the ligands.

removal of the classical water molecules induces a delocalization of the excited electron over different bipyridine ligands.

The excited state chosen to start the dynamics were selected according to their oscillator strength. A first trajectory was initiated from a geometry obtained from the equilibrated QM/MM trajectory. A characterization of its first seven excited states is given in Table 1. The highest oscillator strength belongs to the ^{1}MLCT state S_6, which has a LR-TDDFT excitation energy of 2.125 eV in good agreement with the absorption spectra obtained experimentally [77]. A second trajectory was computed starting from a different configuration. The corresponding excited state assignments follow the previous description, with the exception of an inversion of the states S_5 and S_6, the former having the largest oscillator strength.

4.3. Nonadiabatic dynamics and ^{1}MLCT/^{3}MLCT crossings

Fig. 2 shows the time evolution of the most relevant excited states energies computed along the two selected trajectories. In the first run (left panel of Fig. 2), we observe a surface hop from S_6 to S_5 within the first femtoseconds. These two states are indeed close in energy since the beginning of the dynamics (see Table 1). The system remains in S_5 for more than 25 fs, before a jump occurs first to S_4 and then finally to S_2. This fast relaxation to S_2 leaves no time for important structural changes, both intramolecular to the $[Ru(bpy)_3]^{2+}$ complex, as well as in the surrounding water molecules. However, some fast rearrangements occur in the first solvation shell, leading to a stabilization of the charge localized on one ligand. A comparison between the initial frame and a later one (at time t = 46 fs) clearly shows the ultrafast rearrangement of a single water molecule, which reorients its dipole towards the charged ligand stabilizing the excited state (yellow water molecule in Fig. 3). It is therefore important to explicitly describe at least the first shells of water molecules surrounding the complex in order to be able to capture this fast and important rearrangement of the solvent.

Table 1
First singlet excited states of $[Ru(bpy)_3]^{2+}$ at the initial geometry of the nonadiabatic dynamics obtained with LR-TDDFT/TDA/BP. Only major contributions (>25%) to the excitations are reported.

Singlet state S_n	Excitation energy (eV)	Oscillator strength	Assignment
1	1.557	0.00081	HOMO → LUMO (99.4%)
2	1.709	0.00019	HOMO → LUMO + 1 (98.9%)
3	1.888	0.00226	HOMO-1 → LUMO (84.7%)
4	1.992	0.00453	HOMO-2 → LUMO (35.6%) HOMO-1 → LUMO + 1 (34.6%)
5	2.099	0.00149	HOMO → LUMO + 2 (89.1%)
6	2.125	0.01847	HOMO-2 → LUMO (30.7%) HOMO-1 → LUMO + 1 (28.6%)
7	2.205	0.01500	HOMO → LUMO + 3 (72.9%)

In the second nonadiabatic run (right panel of Fig. 2), the dynamics is initiated in state S_5. The ruthenium complex stays in this initial state for about 20 fs before reaching S_4 through a nonadiabatic surface hop. The trajectory is then propagated with the forces obtained from S_4 during about 20 fs, until a hop to S_3 occurs, followed rapidly (within ~2 fs) by a final jump into S_2.

It is interesting to note that for both trajectories the electronic state S_2 is driving a rather fast relaxation towards the ground state. However, since our interest is focused on early ultrafast ^{1}MLCT/^{3}MLCT crossing events, we decided to stop our trajectories after the state S_2 is reached and strong ^{1}MLCT/^{3}MLCT crossings are observed.

In order to estimate the probability for the ISC between the ^{1}MLCT and the ^{3}MLCT states, we also computed seven triplet excited state energies along the two trajectories reported in Fig. 2. In both cases, we observe that the driving state (blue circles in Fig. 2) crosses different triplet states at different times. Therefore, following the same qualitative arguments exposed above, we should be able, based on the orbital symmetry of the electronic states involved, to predict the size of the SOC matrix elements (at least qualitatively) and therefore gain insights about the probability of the ISCs.

4.4. Analysis of the SOCs at ^{1}MLCT/^{3}MLCT crossings

For the first trajectory (left panel of Fig. 2), the first two crossing events observed between states S_5 and T_7 (white circles in Fig. 2) are expected to exhibit a very small SOC and thus an inefficient ISC. In fact, the two states involved (singlet and triplet) do not

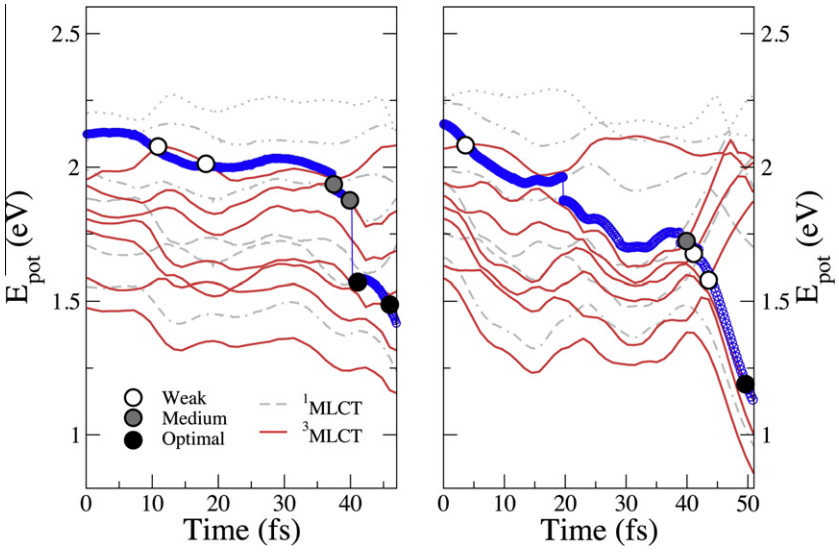

Fig. 2. Nonadiabatic molecular dynamics of $[Ru(bpy)_3]^{2+}$ in solution. In the two panels, we report the time series of the relevant excited state energies for the two trajectories discussed in the text. Singlet excited states (7 in total) are represented by gray dashed lines, triplet states (7 in total) by red continuous lines. The driving state is highlighted with blue circles. Analyzed crossings between singlet and triplet states (see main text) are represented by filled circles with the following color coding: white = weak, gray = medium, and black = optimal SOC strength. (For interpretation of the references to colour in this figure legend, the reader is referred to the web version of this article.)

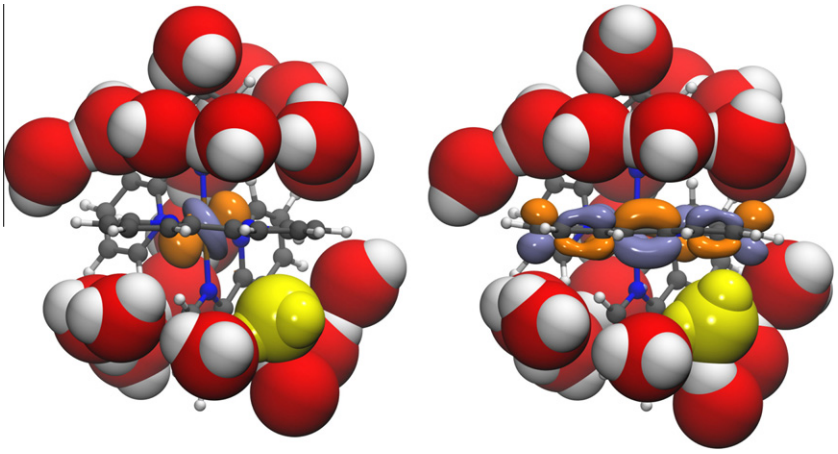

Fig. 3. Ball and stick representation of the $[Ru(bpy)_3]^{2+}$ complex together with part of the first solvation shell of water molecules (van der Waals representation). The selected frames ($t = 0$ fs on the left and $t = 46$ fs on the right) show the fast rotation of a classical water molecule (in yellow) occurring during the dynamics. The molecular orbitals represent the KS-HOMO of the ground state (left) and the populated ligand orbital in S_2 (right). Color code as in Fig. 1 (For interpretation of the references to colour in this figure legend, the reader is referred to the web version of this article.)

share the same π^* ligand-based orbital suggesting a vanishing SOC (see Table 2 and Fig. 1). Concerning the two subsequent crossings between the driving singlet state and the triplet state T_6, a moderate ISC is expected in this case. Indeed, if we consider the coupling between S_5 (main contribution: HOMO-1 → LUMO (59.3%)) and T_6 (HOMO-2 → LUMO (87.4%)), the corresponding orbital symmetry suggests non-vanishing SOC (Table 2 and Fig. 1). The two final crossings (black circles in Fig. 2) occur at structures with optimal electronic configurations that produce large SOC values. The first event consists of a transition between states S_2 and T_4, which are characterized by the single electron transitions HOMO-1 → LUMO + 1 (82.2%) and HOMO-2 → LUMO + 1 (83.1%), respectively.

Table 2
Crossings between ^{1}MLCT and ^{3}MLCT states of $[Ru(bpy)_3]^{2+}$ along the computed trajectories (left panel of Fig. 2). Assignments are indicated with respect to the molecular orbitals shown in Fig. 1.

Time (fs)	Assignment S_n	Assignment T_n
	First trajectory	
10.9	**S_5**	**T_7**
	HOMO-1 → LUMO + 1 (45.1%)	HOMO → LUMO + 2 (95.7%)
	HOMO-2 → LUMO (33.1%)	
18.1	**S_5**	**T_7**
	HOMO-1 → LUMO + 1 (37.8%)	HOMO → LUMO + 2 (95.7%)
	HOMO-2 → LUMO (37.6%)	
37.5	**S_5**	**T_6**
	HOMO-1 → LUMO (59.3%)	HOMO-2 → LUMO (87.4%)
40.0	**S_4**	**T_6**
	HOMO-1 → LUMO (57.3%)	HOMO-2 → LUMO (88.8%)
41.1	**S_2**	**T_4**
	HOMO-1 → LUMO + 1 (82.2%)	HOMO-2 → LUMO + 1 (83.1%)
46.0	**S_2**	**T_3**
	HOMO-1 → LUMO + 1 (84.3%)	HOMO-2 → LUMO + 1 (85.7%)
	Second trajectory	
3.6	**S_5**	**T_7**
	HOMO-2 → LUMO (61.1%)	HOMO → LUMO + 3 (50.9%)
	HOMO-1 → LUMO + 1 (19.9%)	HOMO → LUMO + 2 (43.9%)
39.9	**S_3**	**T_6**
	HOMO-1 → LUMO (84.4%)	HOMO-2 → LUMO (40.8%)
		HOMO-2 → LUMO + 1 (34.3%)
		HOMO-1 → LUMO + 1 (23.9%)
41.1	**S_3**	**T_5**
	HOMO-1 → LUMO (85.2%)	HOMO-1 → LUMO + 1 (78.8%)
43.5	**S_2**	**T_4**
	HOMO-1 → LUMO (97.0%)	HOMO → LUMO + 1 (92.7%)
49.6	**S_2**	**T_3**
	HOMO-1 → LUMO (99.3%)	HOMO-2 → LUMO (98.1%)

Similarly, the second ISC occurs between two states that show a large LUMO + 1 character: S_2 (HOMO-1 → LUMO + 1, 84.3%) and T_3 (HOMO-2 → LUMO + 1, 85.7%). Because of the large overlap given by the common acceptor LUMO + 1 orbital (π^* orbital localized on a single ligand) in this case we can expect, according to Ref. [87], a sizeable SOC and therefore an efficient ISC.

In order to validate these predictions, we computed for the crossing at time $t = 41$ fs (Fig. 1, left panel) the SOC within LR-TDDFT using the perturbative approach by Ziegler and coworkers [64] (see Section 3). This calculation gives indeed a significant SOC splitting of about 400 cm^{-1} (0.05 eV) at singlet–triplet degeneracy, confirming our qualitative analysis based on the symmetry of the orbitals.

The second trajectory (Fig. 1, right panel) reproduces qualitatively the same behavior. The system relaxes from state S_5 to state S_2 within ~40 fs crossing several triple states. Once in S_2, we again observe a strong relaxation towards the ground state and crossings with low energy triplet states with high SOCs.

Concerning the characteristic time scales for the ^{1}MLCT/^{3}MLCT transition, experimental evidence suggests an upper limit of about 300 fs [74,75], while more recent data have shifted this value down to ~15 ± 10 fs [77]. In our simulations we observe strong SOCs between singlet and triplet states occurring within the first 40–50 fs of dynamics. As suggested previously [77], we observe high values of the SOCs when the excited electron is mainly localized on a single ligand.

The dynamics of the ^{3}MLCT $[Ru(bpy)_3]^{2+}$complex in water was the subject of a recent theoretical investigation [58] that stressed the importance of having an atomistic description of the solvent molecules in order to correctly reproduce the complex solvent–solute interactions that drive the localization/delocalization of the unpaired electron in the ligand system. In this study, we observe a very similar behavior for the ^{1}MLCT dynamics. The first solvation shell consists of a long chain of water molecules that intercalate between the ligands (Fig. 4). After excitation, the unpaired electron in the ligand system is stabilized by a sudden reorganization of the water molecules (Fig. 3) [58].

We conclude by mentioning that a complete account of the complex nonadiabatic dynamics of solvated $[Ru(bpy)_3]^{2+}$ would require the calculation of a much larger number of trajectories. However, it is beyond the scope of this paper to produce a fully converged statistical description of this photophysical process. We believe that our results provide interesting insights into the atomistic mechanism underlying this class of ultrafast processes

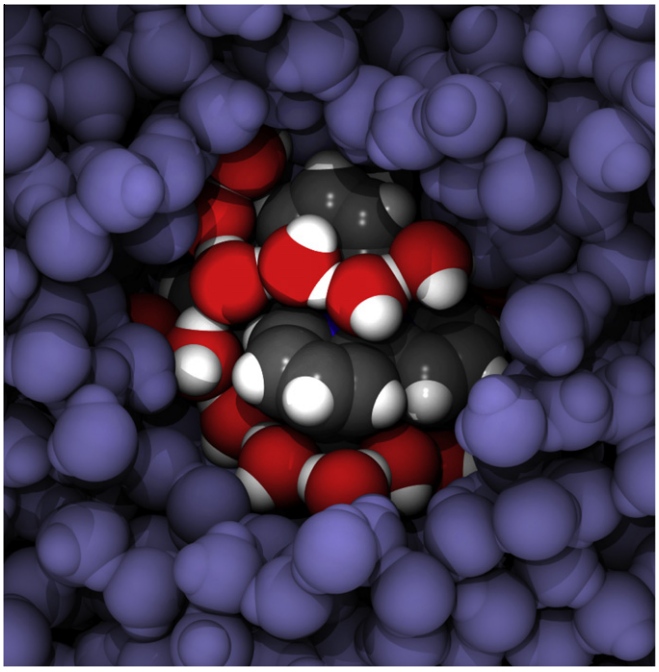

Fig. 4. Snapshot of the QM/MM nonadiabatic molecular dynamics of $[Ru(bpy)_3]^{2+}$ in classical water molecules. Water molecules in a radius of 6.6 Å are represented by the respective van der Waals radius and color of their atoms (oxygens are in red and hydrogens in white). Further solvation water molecules are shown in blue. $[Ru(bpy)_3]^{2+}$ is also represented with vdW spheres. Color code as in Fig. 1. (For interpretation of the references to colour in this figure legend, the reader is referred to the web version of this article.)

and shed new lights on the way ^{1}MLCT/^{3}MLCT ISCs can occur in the femtosecond time scale.

5. Conclusions

In this paper we extended the TSH nonadiabatic dynamics proposed in Ref. [36] to the case of a quantum system coupled to an environment described at a classical molecular mechanics level. All quantities required for the propagation of the nuclei (excited state energies and forces) and for the time evolution of the Tully's TSH amplitudes (NACs and NACVs) are computed at the same level of theory using LR-TDDFT. The coupling of the quantum system to the environment was built into the previously developed QM/MM interface for ground state simulations. This is based on a Hamiltonian additive coupling scheme [51], which naturally includes polarization effects induced by the classical point charges on the quantum subsystem. The excited state density required for the coupling Hamiltonian is computed within both Casida's and Sternheimer's formulation of the LR-TDDFT equations.

As an application of this new scheme, we simulated the ultrafast dynamics of the $[Ru(bpy)_3]^{2+}$ complex in aqueous solution. Starting from the first ^{1}MLCT state with large oscillator strength, we computed the relaxation dynamics of the system looking at the crossings with the lower lying triplet MLCT states. Using a qualitative estimation of the SOCs based on orbital symmetries, we were able to show that several ISC events can already take place within the first 40–50 fs of dynamics, in good agreement with recent experiments [74–77]. The largest couplings were predicted between the lowest energy singlet MLCT states and the corresponding isoenergetic triplet states. This study also emphasizes the important role played by the solvent in the relaxation process in agreement with previous theoretical studies [57,58]. We believe therefore that a full atomistic description of the environment (solvent) together with a proper coupling with the quantum subsystem are essential ingredients for the correct description of photophysical and photochemical processes in solution.

Acknowledgements

The authors thank Majed Chergui and Andrea Cannizzo for useful discussions and the CADMOS project for the computer time on the IBM BlueGene/P. COST action CM0702, Swiss NSF grant 200020-130082, and the NCCR-MUST interdisciplinary research program are acknowledged for fundings. We also thank Jürg Hutter for the help in the implementation of the LR-TDDFT/MM interface in the CPMD package.

Appendix A

In this Appendix we give a short summary of the derivation of the response density matrix within the Sternheimer formalism [21].

Expanding the ground state KS orbitals, $\{\phi_i(\mathbf{r})\}$, and the linear response orbitals $\{\phi_i^{\{\pm\}}(\mathbf{r})\}$ in an orthogonal basis set $\{\kappa_p(\mathbf{r})\}$ defines the expansion coefficients $\left\{c_{pi}^{\{0\}}\right\}$ and $\left\{c_{pi}^{\{\pm\}}\right\}$

$$\phi_i(\mathbf{r}) = \sum_{p=1}^{M} c_{pi}^{\{0\}} \kappa_p(\mathbf{r}),$$
$$\phi_i^{\{\pm\}}(\mathbf{r}) = \sum_{p=1}^{M} c_{pi}^{\{\pm\}} \kappa_p(\mathbf{r}). \tag{27}$$

In the following, the indices $i, j, k, \ldots$ run over the KS states $(1,\ldots,N)$, and the indices $p, q, r, \ldots$ refer to the basis functions $(1,\ldots,M)$. In order to simplify the notation, we drop the index I that labels the linear response solutions for the different excited states.

Introducing the new set of coefficients

$$x_{pi} = \frac{1}{2}\left(c_{pi}^{\{+\}} + c_{pi}^{\{-\}}\right),$$
$$y_{pi} = \frac{1}{2}\left(c_{pi}^{\{+\}} - c_{pi}^{\{-\}}\right). \tag{28}$$

Eq. (25) can be recast as

$$\mathcal{A}(\mathcal{A}+\mathcal{B})\mathbf{x} = \omega^2\mathbf{x}, \tag{29}$$
$$(\mathcal{A}+\mathcal{B})\mathcal{A}\mathbf{y} = \omega^2\mathbf{y}. \tag{30}$$

The (super-)operators $\mathcal{A}$ and $\mathcal{B}$ are defined as

$$\mathcal{A}_{pi,qj} = \mathbf{F}_{pq}\delta_{ij} - \epsilon_{ij}\delta_{pq}, \tag{31}$$
$$\mathcal{B}_{pi,qj} = \sum_{rsuv} \mathbf{Q}_{pr} c_{ui}^{\{0\}} \mathcal{K}_{ru,sv} \left(c_{vj}^{\{0\}}\right)^* \mathbf{Q}_{sq}, \tag{32}$$

where

$$\mathbf{F}_{pq} = \langle \kappa_p | \mathcal{H}_0 | \kappa_q \rangle, \tag{33}$$
$$\epsilon_{ij} = \sum_{pq} \left(c_{pi}^{\{0\}}\right)^* \mathbf{F}_{pq} c_{qj}^{\{0\}}, \tag{34}$$
$$\mathbf{P}_{pq} = \sum_{i} c_{pi}^{\{0\}} \left(c_{qi}^{\{0\}}\right)^*, \tag{35}$$
$$\mathbf{Q}_{pq} = \delta_{pq} - \mathbf{P}_{pq}, \tag{36}$$
$$\mathcal{K}_{pu,qv} = \int d\mathbf{r} \int d\mathbf{r}' \kappa_p^*(\mathbf{r}) \kappa_u(\mathbf{r}) \left[\frac{1}{|\mathbf{r}-\mathbf{r}'|} + \left.\frac{\delta^2 E_{xc}}{\delta\rho(\mathbf{r})\delta\rho(\mathbf{r}')}\right|_{\rho=\rho_0}\right] \kappa_v^*(\mathbf{r}') \kappa_q(\mathbf{r}'). \tag{37}$$

Within this framework, the response density matrix elements in TDA are given by the expression [21]

$$\Delta P_{pq} = \sum_i x_{qi} x_{pi}^* + \sum_{rij} x_{rj} c_{pj}^{\{0\}} \left(c_{qi}^{\{0\}}\right)^* (x_{ri})^*. \tag{38}$$

References

[1] E. Runge, E.K.U. Gross, Phys. Rev. Lett. 52 (1984) 997.
[2] E.K.U. Gross, W. Kohn, Phys. Rev. Lett. 55 (1985) 2850.
[3] M.E. Casida, Time-dependent density-functional response theory for molecules, in: D.P. Chong (Ed.), Recent Advances in Density Functional Methods, World Scientific, Singapore, 1995, p. 155.
[4] M. Petersilka, U.J. Gossmann, E.K.U. Gross, Phys. Rev. Lett. 76 (1996) 1212.
[5] H. Appel, E.K.U. Gross, K. Burke, Phys. Rev. Lett. 90 (2003) 043005.
[6] H. Lischka, R. Shepard, I. Shavitt, R.M. Pitzer, M. Dallos, T. Mller, P.G. Szalay, F.B. Brown, R. Ahlrichs, H.J. Bhm, A. Chang, D.C. Comeau, R. Gdanitz, H. Dachsel, C. Ehrhardt, M. Ernzerhof, P. Hchtl, S. Irle, G. Kedziora, T. Kovar, V. Parasuk, M.J.M. Pepper, P. Scharf, H. Schiffer, M. Schindler, M. Schler, M. Seth, E.A. Stahlberg, J.-G. Zhao, S. Yabushita, Z. Zhang, M. Barbatti, S. Matsika, M. Schuurmann, D.R. Yarkony, S.R. Brozell, E.V. Beck, J.-P. Blaudeau, COLUMBUS, an ab initio electronic structure program, release 5.9.1, 2006.
[7] A.J.A. Aquino, H. Lischka, J. Chem. Phys. A 109 (2005) 3201.
[8] P. Wiggins, J.A.G. Williams, D.J. Tozer, J. Chem. Phys. 131 (9) (2009) 091101.
[9] J. Neugebauer, E.J. Baerends, M. Nooijen, J. Chem. Phys. 121 (2004) 6155.
[10] K. Giesbertz, E. Baerends, Chem. Phys. Lett. 461 (2008) 338.
[11] M.A.L. Marques, C.A. Ullrich, F. Nogueira, A. Rubio, K. Burke, E.K.U. Gross (Eds.), Time-Dependent Density Functional Theory, Lecture Notes of Physics, Springer, Berlin, 2006.
[12] T. Yanai, D. Tew, N. Handy, Chem. Phys. Lett. 393 (2004) 51.
[13] Y. Tawada, T. Tsuneda, S. Yanagisawa, T. Yanai, K. Hirao, J. Chem. Phys. 120 (2004) 8425.
[14] O.A. Vydrov, G.E. Scuseria, J. Chem. Phys. 125 (2006) 234109.
[15] Y. Zhao, D.G. Truhlar, Theor. Chem. Acc. 120 (2008) 215.
[16] Y. Zhao, D.G. Truhlar, Acc. Chem. Res. 41 (2) (2008) 157.
[17] D. Jacquemin, E.A. Perpete, G. Scalmani, M.J. Frisch, R. Kobayashi, C. Adamo, J. Chem. Phys. 126 (14) (2007) 144105.
[18] K. Nguyen, P. Day, R. Pachter, Theor. Chem. Accounts: Theory, Comput. Model. (Theor. Chim. Acta) 120 (2008) 167.
[19] J. Plotner, D.J. Tozer, A. Dreuw, J. Chem. Theory Comput. 6 (8) (2010) 2315.
[20] F. Furche, R. Ahlrichs, J. Chem. Phys. 117 (2002) 7433.
[21] J. Hutter, J. Chem. Phys. 118 (2003) 3928.
[22] L.D. Landau, Phys. Z. Sowjetunion 2 (1932) 46.
[23] C. Zener, Proc. Roy. Soc. Lond., Ser. A 137 (1932) 696.
[24] E.C.G. Stueckelberg, Helv. Phys. Acta 5 (1932) 369.
[25] J.C. Tully, J. Chem. Phys. 93 (1990) 1061.
[26] P. Ehrenfest, Z. Phys. 45 (1927) 455.
[27] B.F.E. Curchod, I. Tavernelli, U. Rothlisberger, Phys. Chem. Chem. Phys. 13 (2011) 3231.
[28] S.R. Mercier, O.V. Boyarkin, A. Kamariotis, M. Guglielmi, I. Tavernelli, M. Cascella, U. Rothlisberger, T. Rizzo, J. Am. Chem. Soc. 128 (2006) 16938.
[29] M. Guglielmi, I. Tavernelli, U. Rothlisberger, Phys. Chem. Chem. Phys. 11 (2009) 4549.
[30] E. Tapavicza, I. Tavernelli, U. Rothlisberger, C. Filippi, M.E. Casida, J. Chem. Phys. 129 (2008) 124108.
[31] I. Tavernelli, Phys. Rev. B 73 (2006) 094204.
[32] I. Tavernelli, M.-P. Gaigeot, R. Vuilleumier, C. Stia, M.-A. Herv du Penhoat, M.-F. Politis, Chem. Phys. Chem. 9 (14) (2008) 2099.
[33] V. Chernyak, S. Mukamel, J. Chem. Phys. 112 (2000) 3572.
[34] R. Baer, Chem. Phys. Lett. 364 (2002) 75.
[35] J. Neugebauer, E.J. Baerends, M. Nooijen, J. Phys. Chem. A 109 (2005) 1168.
[36] E. Tapavicza, I. Tavernelli, U. Rothlisberger, Phys. Rev. Lett. 98 (2007) 023001.
[37] I. Tavernelli, E. Tapavicza, U. Rothlisberger, J. Chem. Phys. 130 (2009) 124107.
[38] I. Tavernelli, E. Tapavicza, U. Rothlisberger, J. Mol. Struct. (Theochem.) 914 (2009) 22.
[39] C.P. Hu, H. Hirai, O. Sugino, J. Chem. Phys. 127 (2007) 064103.
[40] I. Tavernelli, B.F.E. Curchod, U. Rothlisberger, J. Chem. Phys. 131 (2009) 196101.
[41] I. Tavernelli, B.F.E. Curchod, A. Laktionov, U. Rothlisberger, J. Chem. Phys. 133 (2010) 194104.
[42] M. Thachuk, M.Y. Ivanov, D.M. Wardlaw, J. Chem. Phys. 109 (1998) 5747.
[43] J.Y. Fang, S. Hammes-Schiffer, J. Phys. Chem. A 103 (1999) 9399.
[44] G. Granucci, M. Persico, J. Chem. Phys. 126 (2007). 134114-11.
[45] M. Barbatti, R. Shepard, H. Lischka, Computational and methodological elements for nonadiabatic trajectory dynamics simulations of molecules, in: W. Domcke, D.R. Yarkony, H. Koeppel (Eds.), Conical Intersections: Theory, Computation and Experiment, World Scientific, Singapore, 2010, in press.
[46] I. Tavernelli, B.F.E. Curchod, U. Rothlisberger, Phys. Rev. A 81 (2010) 052508.
[47] CPMD, Copyright IBM Corp 1990-2001, Copyright MPI für Festkörperforschung Stuttgart, 1997–2001, <http://www.cpmd.org>.
[48] S. Tretiak, S. Mukamel, Chem. Rev. 102 (9) (2002) 3171.
[49] A. Fetter, J. Walecka, Quantum Theory of Many-Particle Systems, McGraw-Hill, New York, 1971.
[50] A. Laio, J. VandeVondele, U. Rothlisberger, J. Phys. Chem. B 106 (2002) 7300.
[51] A. Laio, J. VandeVondele, U. Rothlisberger, J. Chem. Phys. 116 (16) (2002) 6941.
[52] U. Rothlisberger, P. Carloni, Lect. Notes Phys. 704 (2006) 437.
[53] M.E. Moret, E. Tapavicza, L. Guidoni, U.F. Röhrig, M. Sulpizi, I. Tavernelli, U. Rothlisberger, Chimia 59 (2005) 493.
[54] M.E. Casida, J. Mol. Struct.: THEOCHEM 914 (1–3) (2009) 3–18, time-dependent density-functional theory for molecules and molecular solids.
[55] A. Ipatov, F. Cordova, L.J. Doriol, M.E. Casida, J. Mol. Struct.: THEOCHEM 914 (1–3) (2009) 60–73, time-dependent density-functional theory for molecules and molecular solids.
[56] R. Sternheimer, Phys. Rev. 84 (2) (1951) 244.
[57] M.-E. Moret, I. Tavernelli, U. Rothlisberger, J. Phys. Chem. B 113 (22) (2009) 7737.
[58] M.-E. Moret, I. Tavernelli, M. Chergui, U. Rothlisberger, Chem. Eur. J. 16 (20) (2010) 5889.
[59] A.D. Becke, Phys. Rev. A 38 (1988) 3098.
[60] Perdew, Phys. Rev. B Condens. Matter 33 (12) (1986) 8822.
[61] N. Troullier, J.L. Martins, Phys. Rev. B 43 (1991) 1993.
[62] M.J. Frisch, G.W. Trucks, H.B. Schlegel, G.E. Scuseria, M.A. Robb, J.R. Cheeseman, G. Scalmani, V. Barone, B. Mennucci, G.A. Petersson, H. Nakatsuji, M. Caricato, X. Li, H.P. Hratchian, A.F. Izmaylov, J. Bloino, G. Zheng, J.L. Sonnenberg, M. Hada, M. Ehara, K. Toyota, R. Fukuda, J. Hasegawa, M. Ishida, T. Nakajima, Y. Honda, O. Kitao, H. Nakai, T. Vreven, J.A. Montgomery, Jr., J.E. Peralta, F. Ogliaro, M. Bearpark, J.J. Heyd, E. Brothers, K.N. Kudin, V.N. Staroverov, R. Kobayashi, J. Normand, K. Raghavachari, A. Rendell, J.C. Burant, S.S. Iyengar, J. Tomasi, M. Cossi, N. Rega, J.M. Millam, M. Klene, J.E. Knox, J.B. Cross, V. Bakken, C. Adamo, J. Jaramillo, R. Gomperts, R.E. Stratmann, O. Yazyev, A.J. Austin, R. Cammi, C. Pomelli, J.W. Ochterski, R.L. Martin, K. Morokuma, V.G. Zakrzewski, G.A. Voth, P. Salvador, J.J. Dannenberg, S. Dapprich, A.D. Daniels,. Farkas, J.B. Foresman, J.V. Ortiz, J. Cioslowski, D.J. Fox, Gaussian 09, Revision A.1, Gaussian Inc., Wall.
[63] F. Alary, J.-L. Heully, L. Bijeire, P. Vicendo, Inorg. Chem. 46 (8) (2007) 3154.
[64] F. Wang, T. Ziegler, J. Chem. Phys. 123 (15) (2005) 154102.
[65] C.F. Guerra, J. Snijders, G. te Velde, E. Baerends, Theor. Chem. Acc. 99 (1998) 391.
[66] S. van Gisbergen, J. Snijders, E. Baerends, Comput. Phys. Commun. 118 (1999) 119.
[67] G. te Velde, F. Bickelhaupt, S. van Gisbergen, C.F. Guerra, E. Baerends, J. Snijders, T. Ziegler, J. Comput. Chem. 22 (2001) 931.
[68] ADF2009.01, SCM, Theoretical Chemistry, Vrije Universiteit, Amsterdam, The Netherlands, <http://www.scm.com>, 2009.
[69] E. van Lenthe, E. Baerends, J. Snijders, J. Chem. Phys. 99 (1993) 4597.
[70] E. van Lenthe, E. Baerends, J. Snijders, J. Chem. Phys. 101 (1994) 9783.
[71] C. Pye, T. Ziegler, Theor. Chem. Acc. 101 (1999) 396.
[72] It is important to mention that the implicit solvent calculations were performed with different software packages (Gaussian09 and ADF2009) using localized basis sets.
[73] W. Humphrey, A. Dalke, K. Schulten, J. Mol. Graph 14 (1996) 33.
[74] N.H. Damrauer, G. Cerullo, A. Yeh, T.R. Boussie, C.V. Shank, J.K. McCusker, Science 275 (5296) (1997) 54.
[75] A.T. Yeh, C.V. Shank, J.K. McCusker, Science 289 (5481) (2000) 935.
[76] W. Gawelda, M. Johnson, F.M.F. de Groot, R. Abela, C. Bressler, M. Chergui, J. Am. Chem. Soc. 128 (2006) 5001.
[77] A. Cannizzo, F. van Mourik, W. Gawelda, G. Zgrablic, C. Bressler, M. Chergui, Angew. Chem. Int. Ed. 45 (2006) 3174.
[78] M. Buchs, C. Daul, CHIMIA Int. J. Chem. 52 (1998) 163. 4.
[79] J.-L. Heully, F. Alary, M. Boggio-Pasqua, J. Chem. Phys. 131 (2009) 184308.
[80] I. Tunell, Z. Rinkevicius, O. Vahtras, P. Salek, T. Helgaker, H. Agren, J. Chem. Phys. 119 (21) (2003) 11024.
[81] B. Minaev, I. Tunell, P. Salek, O. Loboda, O. Vahtras, H. gren, Mol. Phys. 102 (13) (2004) 1391.
[82] F. Wang, T. Ziegler, E. van Lenthe, S. van Gisbergen, E.J. Baerends, J. Chem. Phys. 122 (20) (2005) 204103.
[83] F. Wang, T. Ziegler, J. Chem. Phys. 123 (19) (2005) 194102.
[84] C. Carbogno, J. Behler, K. Reuter, A. Groß, Phys. Rev. B 81 (3) (2010) 035410.
[85] F.D. Angelis, L. Belpassi, S. Fantacci, J. Mol. Struct.: THEOCHEM 914 (1–3) (2009) 74–86. time-dependent density-functional theory for molecules and molecular solids.
[86] T. Bessho, E. Yoneda, J.-H. Yum, M. Guglielmi, I. Tavernelli, H. Imai, U. Rothlisberger, M.K. Nazeeruddin, M. Grätzel, J. Am. Chem. Soc. 131 (16) (2009) 5930.
[87] A.F. Rausch, H.H.H. Homeier, H. Yersin, Top Organomet Chem, Springer-Verlag, Berlin, Heidelberg, 2009. Chapter: Organometallic Pt(II) and Ir(III) Triplet Emitters for OLED Applications and the Role of Spin-Orbit Coupling: A Study Based on High-Resolution Optical Spectroscopy, pp. 193–235.